

---

# Expression and characterization of soluble amino-terminal domain of NR2B subunit of N-methyl-D-aspartate receptor

---

ESTHER WONG,<sup>1,4</sup> FUI-MEE NG,<sup>2,4</sup> CHYE-YUN YU,<sup>1</sup> PEIQI LIM,<sup>1,2</sup>  
LENG-HIONG LIM,<sup>1</sup> STEPHEN F. TRAYNELIS,<sup>3</sup> AND CHIAN-MING LOW<sup>1,2</sup>

<sup>1</sup>Glutamate Receptor Laboratory, National Neuroscience Institute, S308433, Singapore

<sup>2</sup>Department of Pharmacology, National University of Singapore, S117597, Singapore

<sup>3</sup>Department of Pharmacology, Emory University School of Medicine, Atlanta, Georgia 30322-3090, USA

(RECEIVED April 11, 2005; FINAL REVISION May 30, 2005; ACCEPTED May 30, 2005)

## Abstract

N-methyl-D-aspartate (NMDA) receptors are involved in mediating excitatory synaptic transmissions in the brain and have been implicated in numerous neurologic disorders. The proximal amino-terminal domains (ATDs) of NMDA receptors constitute many modulatory binding sites that may serve as potential drug targets. There are few biochemical and structural data on the ATDs of NMDA receptors, as it is difficult to produce the functional proteins. Here an optimized method was established to reconstitute the insoluble recombinant ATD of NMDA receptor NR2B subunit (ATD2B) through productive refolding of 6xHis-ATD2B protein from inclusion bodies. Circular dichroism and dynamic light scattering characterizations revealed that the solubilized and refolded 6xHis-ATD2B adopted well-defined secondary structures and monodispersity. More significantly, the soluble 6xHis-ATD2B specifically bound ifenprodil to saturation. Ifenprodil bound to 6xHis-ATD2B with a dissociation constant ( $K_D$ ) of  $127.5 \pm 45$  nM, which was within the range of the  $IC_{50}$  determined electrophysiologically. This is the first report on a functional recombinant ATD2B with a characterized  $K_D$ .

**Keywords:** NR2B NMDA receptor; protein refolding; circular dichroism; dissociation constant; dynamic light scattering

N-methyl-D-aspartate (NMDA) receptors are ligand-gated ion channels that exhibit voltage-dependent  $Mg^{2+}$  channel block. Under physiological conditions, NMDA receptors

play vital roles in excitatory synaptic transmission, synaptic plasticity, learning, and memory formation as well as neuronal development (Dingledine et al. 1999). However, overactivation of these receptors can cause excessive  $Ca^{2+}$  influx into the neurons, leading to excitotoxic neuronal cell death associated with ischemic stroke (Dirnagl et al. 1999; Lee et al. 1999) and head trauma (Obrenovitch and Urenjak 1997). The causative role of NMDA receptors has also been implicated in seizures (Meldrum et al. 1999). As such, NMDA receptors can be potential targets for therapeutic intervention in these pathological situations.

The NMDA receptor consists of a complex of four or five subunits that include an obligatory NR1 subunit together with the NR2A-D or NR3A-B subunits (Dingledine et al. 1999). The architecture of each

---

<sup>4</sup>These authors contributed equally to this work.

Reprint requests to: Chian-Ming Low, Department of Pharmacology, MD2 #04-22, Faculty of Medicine, National University of Singapore, 18 Medical Drive, S117597, Singapore; e-mail: phclowcm@nus.edu.sg; fax: +(65) 68737690.

**Abbreviations:** NMDA, N-methyl-D-aspartate; ATD, amino-terminal domain; CD, circular dichroism; DLS, dynamic light scattering;  $K_D$ , dissociation constant; LIVBP, leucine/isoleucine/valine-binding protein; MALDI-TOF, matrix-assisted laser desorption ionization time of flight; MS, mass spectrometry.

Article and publication are at <http://www.protein-science.org/cgi/doi/10.1110/ps.051509905>.

NMDA receptor subunit is organized in a modular fashion: an amino-terminal domain (ATD), a ligand-binding domain (S1S2), three transmembrane domains (TM-I, -III and -IV), a re-entrant pore loop (initially identified as TM-II), and a carboxy-terminal domain (Wo and Oswald 1995; Paas 1998). The extracellular ATD, defined by the first ~400 amino acids, exhibits structural homology to a family of bacterial periplasmic amino acid-binding proteins (PBPs), especially the leucine/isoleucine/valine-binding protein (LIVBP) (Nakanishi et al. 1990). Although the ATD of NMDA receptor is not directly involved in ligand binding, it is implicated in subunit assembly (Meddows et al. 2001; Perez-Otano et al. 2001). More importantly, in the NR2 subunits, the ATD forms or influences the binding site of many NMDA receptor modulators such as protons, polyamines,  $Zn^{2+}$ , and ifenprodil (Gallagher et al. 1996, 1997; Masuko et al. 1999; Low et al. 2000; Paoletti et al. 2000; Perin-Dureau et al. 2002), and influences receptor desensitization (Krupp et al. 1998; Villarroel et al. 1998; Zheng et al. 2001).

Recently the crystal structure of NMDA receptor glycine-binding domain, S1S2 of the NR1 subunit, has been resolved (Furukawa and Gouaux 2003). The structural data of the NR1 S1S2 domain yielded insights into the mechanisms of activation, inhibition, and specificity by antagonist and partial and full agonists. However, the crystal structure of the modulator-binding ATD of ionotropic glutamate receptors is still unknown. Thus far, only the extracellular glutamate-binding domain of metabotropic glutamate receptor subtype 1 (mGluR1), which also shows structural homology to the bacterial LIVBP, has been crystallized (Kunishima et al. 2000). The lack of crystallographic data for apo- and modulator-bound ATDs of NMDA receptors has limited our understanding of the exact binding mechanisms and the molecular determinants involved in binding various modulators.

The lag in the 3D structural data of ATD modulatory domains is partly attributed to the difficulties in obtaining large amounts of soluble native proteins. In this study, we expressed recombinant ATD of NMDA receptor NR2B subunit (ATD2B) as a 6xHis-tagged fusion protein in *Escherichia coli*. Despite high-level expression, the protein accumulated predominantly in the inclusion bodies. It is not uncommon for recombinant membrane receptor domains to be insoluble. The initially insoluble ligand-binding S1S2 domain of ionotropic glutamate receptor, GluR2, was successfully crystallized using proteins reconstituted from the inclusion bodies through denaturation and refolding (Chen and Gouaux 1997). We obtained large amounts of reconstituted 6xHis-ATD2B proteins for structural characterization by employing the same strategy of a fractional factorial folding screen used successfully to determine the best refolding conditions for GluR2 S1S2 (Chen and Gouaux 1997).

Here we report the protocol for overexpression of the proximal 367 amino acids preceding the S1 domain of the NR2B subunit in *E. coli*, one-step purification of Gdn.HCl-extracted 6xHis-ATD2B with a nickel HiTrap chelating metal affinity column, and refolding of 6xHis-ATD2B into soluble protein that binds ifenprodil with a nanomolar  $K_D$  value as determined by circular dichroism (CD) spectroscopy. This functional 6xHis-ATD2B with a defined conformation will greatly facilitate the screening of putative ligands that bind to this domain. Subsequent site-directed mutagenesis of the 6xHis-ATD2B could also be used to identify the molecular determinants that coordinate ligand binding. This 6xHis-ATD2B is thus a valuable tool for further structural and functional studies of NMDA receptors containing the NR2B subunit.

## Results

### *Overexpression of the extracellular domain of the NMDA receptor NR2B subunit*

A high-expression vector, pET30b(+)-EG (Chen and Gouaux 1997), was used to overexpress the 6xHis-ATD2B fusion protein in *E. coli* (Figs. 1, 2). The reading frame encodes the first 367 amino acids (R27–R393) of the amino terminus of the NR2B subunit, preceded by a linker and a 6x-histidine tag (Fig. 1). Four selected colonies of pET30b(+)-EG-ATD2B plasmid transformed *E. coli* were induced in 50 mL of LB with 0.5 mM IPTG for 3 h at 37°C (220 rpm). Bacterial cells were lysed by sonication, and the extracts were separated into soluble (supernatant) and insoluble (inclusion bodies) fractions by centrifugation. Aliquots of these fractions were analyzed by Coomassie brilliant blue-stained 15% SDS-PAGE gels (Fig. 2A). A prominent 6xHis-ATD2B protein band (47 kDa) was detected in all insoluble fractions (>90%) with little or no detectable soluble 6xHis-ATD2B (<10%). The 6xHis-ATD2B proteins were confirmed by immunoblotting with 6xHis antibody and anti-NR2B antibody (Fig. 2B). The highest-expressing 6xHis-ATD2B colony was selected for protein production, although the majority of 6xHis-ATD2B was concentrated in inclusion bodies. The 6xHis-ATD2B was solubilized from its inclusion bodies through denaturation and in vitro refolding.

### *16 refolding matrix screen*

Chen and Gouaux (1997) had successfully used a fractional factorial folding screen to determine the best refolding conditions for the production of active S1S2 ligand binding domain of AMPA receptor. The same screen, involving the systematic examination of 12 factors (protein concentration, pH, ionic strength, divalent cation concentration,

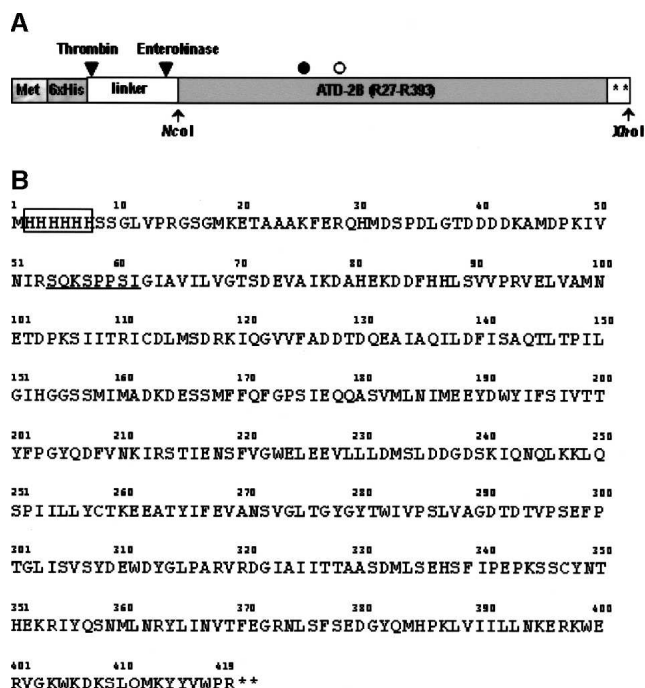


**Figure 1.** Design, construction, and cloning of ATD of NR2B subunit. (A) Schematic representation of the expressed construct of ATD2B with its 6xHis-tag and linker. The DNA fragment between the two arrows was inserted into vector pET30b(+)-EG at the NcoI and XhoI sites. The relative positions of the silent mutations (H127H and L199L) introduced by mutagenesis to abolish the endogenous NcoI (●) and XhoI (○) sites are indicated *above* the gene insert. Proteases cleavage sites are indicated by ▼. (B) Amino acid sequence of 6xHis-ATD2B (419aa; M1H2H3...W417P418R419) expressed from pET30b(+)-EG ATD2B construct. 6xHis-tag is boxed and shaded. Underlined, amino-terminal sequence of thrombin-cleaved 6xHis-ATD2B (Midwest Analytical). Two stop codons (\*) were inserted *after* R393 of the gene insert. The predicted molecular weight of 6xHis-ATD2B is 47,464.2 Da ([http://www.structure.llnl.gov/Xray/comp/comp\\_cell\\_vm.htm#Molecular](http://www.structure.llnl.gov/Xray/comp/comp_cell_vm.htm#Molecular)) and the pI is 4.83 (<http://www.embl-heidelberg.de/cgi/pi-wrapper.pl>).

temperature, ionic additive, nonionic additive, chaotrope, reducing/oxidizing agents, detergent, PEG, and ligand) in a total of 16 experiments was used in the present study to define the parameters required to maximize the yield of monodispersed 6xHis-ATD2B proteins. From our screen, Buffer 13 yielded the highest percentage recovery (92.7%) and the highest monodispersity in terms of monomer:dimer ratio (2.33) (Table 1). Notably, Buffers 9 and 12 yielded the next highest monomer:dimer ratios (1.99 and 1.90, respectively) (Table 1).

#### Purification of 6xHis-ATD2B under denaturing conditions followed by large-scale refolding

Once the refolding condition (Buffer 13) was identified, a scale-up purification and refolding approach using 4 M Gdn.HCl solubilized 6xHis-ATD2B was adopted.

Typically, 30 mg of total solubilized 6xHis-ATD2B protein from 1 L induced *E. coli* culture was loaded into a Ni<sup>2+</sup>-column (HiTrap HP 5 mL, Amersham), and the bound proteins were eluted with 300 mM imidazole. Nine milligrams of the purified 6xHis-ATD2B could be recovered from this one-step affinity purification (30% yield). The resultant protein had purity of ~90% as determined by densitometry (Fig. 2C). The amount of refolded protein obtained from 1 L induction was 3 mg (10% yield of the total solubilized 6xHis-ATD2B). The correct translation of 6xHis-ATD2B was confirmed by amino-terminal protein sequencing (Fig. 1B) of the thrombin-cleaved 6xHis-ATD2B and trypsin-digest MALDI-TOF (matrix-assisted laser desorption ionization-time of flight) mass spectrometry (Table 2) of this protein, respectively. The molecular weight of the Buffer 13 refolded 6xHis-ATD2B protein by MALDI-TOF mass spectrometry was found to be 46,839.3 Da (Fig. 3A), which agrees with the estimated molecular weight of 47,464.2 Da.

#### DLS analyses of Buffer 13-refolded soluble 6xHis-ATD2B

The conformation and binding properties of 6xHis-ATD2B must be determined prior to its applications in

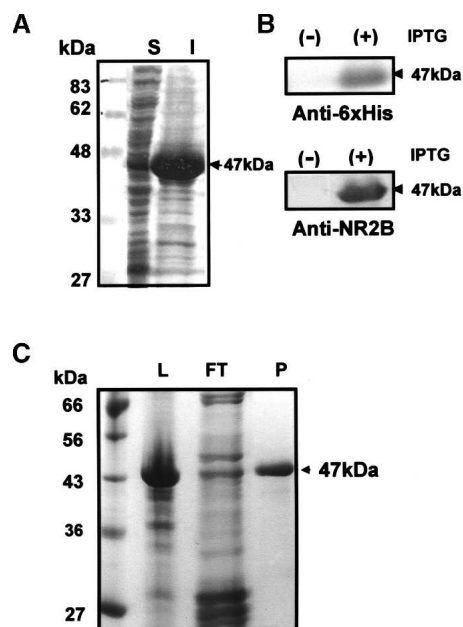


**Figure 2.** Expression and purification of 6xHis-ATD2B. (A) Coomassie blue-stained SDS-PAGE gel showing the soluble (S) and insoluble (I) fractions of the expressed 6xHis-ATD2B. (B) Western blot of the uninduced (-IPTG) and induced (+IPTG) pET30b(+)-EG-ATD2B construct using anti-6xHis (*top*) and anti-NR2B (*bottom*) as primary antibodies. (C) Coomassie blue-stained affinity-purified 6xHis-ATD2B. L, load; FT, flow-through; P, purified 6xHis-ATD2B.

**Table 1.** Fractional factorial folding screen of 6xHis-ATD2B highlighting % recovery and ratio of monomer:dimer

Buffer no.	Protein (mg/ml)	IS <sup>a</sup> pH (mM)	T (°C)	Divalents <sup>b</sup>	Polar additive	Nonpolar additive <sup>c</sup> (%)	Chaotrope	Reduced/oxidized <sup>d</sup>	Detergent (mM) <sup>e</sup>	PEG (%) <sup>f</sup>	Ligand (mM) <sup>g</sup>	Recovery (%)	Ratio of monomers/dimers	
1	0.1	8.5	10	20	Mg/Ca	None	21	None	DTT	5.0	0.05	None	45.9	1.63
2	1.0	8.5	250	4	EDTA	None	None	None	DTT	None	0.05	None	17.8	1.67
3	0.1	8.5	250	20	EDTA	0.5M Arg	None	0.75M Gdn.HCl	DTT	5.0	None	None	100	1.88
4	0.1	8.5	10	4	EDTA	0.5M Arg	None	0.75M Gdn.HCl	GSH:GSSG	None	0.05	10.0	49.9	1.26
5	1.0	6.0	250	4	Mg/Ca	0.5M Arg	None	None	GSH:GSSG	5.0	None	None	80.6	1.65
6	1.0	6.0	250	20	EDTA	None	21	0.75M Gdn.HCl	DTT	None	None	10.0	24.6	1.63
7	1.0	8.5	250	20	Mg/Ca	0.5M Arg	21	0.75M Gdn.HCl	GSH:GSSG	5.0	0.05	10.0	94.7	1.78
8	0.1	6.0	10	4	Mg/Ca	None	None	0.75M Gdn.HCl	DTT	5.0	None	10.0	72.4	1.35
9	1.0	6.0	10	20	Mg/Ca	0.5M Arg	None	None	DTT	None	0.05	10.0	40.4	1.99
10	0.1	6.0	250	4	EDTA	0.5M Arg	21	None	DTT	5.0	0.05	10.0	92.8	1.69
11	0.1	6.0	250	20	Mg/Ca	None	None	0.75M Gdn.HCl	GSH:GSSG	None	0.05	None	64.1	1.64
12	1.0	6.0	10	4	EDTA	None	21	0.75M Gdn.HCl	GSH:GSSG	5.0	0.05	None	62.3	1.90
13	1.0	8.5	10	4	Mg/Ca	0.5M Arg	21	0.75M Gdn.HCl	DTT	None	None	None	92.7	2.33
14	1.0	8.5	10	20	EDTA	None	None	None	GSH:GSSG	5.0	None	10.0	13.2	1.74
15	0.1	8.5	250	4	Mg/Ca	None	21	None	GSH:GSSG	None	None	10.0	42.8	1.77
16	0.1	6.0	10	20	EDTA	0.5M Arg	21	None	GSH:GSSG	None	None	None	84.8	1.73

<sup>a</sup> Ionic strength, 1:25 molar ratio of NaCl to KCl.

<sup>b</sup> MgCl<sub>2</sub>, CaCl<sub>2</sub> concentrations were 2 mM; EDTA concentration was 1.0 mM.

<sup>c</sup> The nonpolar additive consisted of 20% glycerol (v/v) and 1% sucrose (w/v).

<sup>d</sup> Either 1.0 mM DTT or reduced (GSH) and oxidized (GSSG) glutathione in 1.0 and 0.1 mM, respectively.

<sup>e</sup> 1, 2-Diheptanoyl-*sn*-glycero-3-phosphocholine.

<sup>f</sup> PEG, MWave = 3350 Da, (w/v).

<sup>g</sup> Ro 25-6981.

biochemical and crystallographic screens. The soluble proteins obtained after purification, refolding, and concentration exhibited monodispersity at 1 mg/mL (25°C) when studied by dynamic light scattering (DLS) (Fig. 3B). The average hydrodynamic molecular weight of the soluble protein was calculated to be 193 kDa at pH 8.5 (Dynamic V5, Protein Solutions).

#### CD spectroscopy analyses of Buffer 13-refolded soluble 6xHis-ATD2B

CD spectra of 6xHis-ATD2B in a nondenaturing buffer and a denaturing buffer are shown in Figure 4A. Far-UV CD spectrum of Buffer 13-refolded 6xHis-ATD2B corresponded to a trough at 216 nm (Fig. 4A, dotted curve). The relative percentage of  $\alpha$ -helices was estimated to be 26.8%, which is in good agreement with

the values returned from the Hierarchical Neural Net (HNN) Secondary Structure Prediction (25%) ([http://npsa-pbil.ibcp.fr/cgi-bin/secpred\\_hnn.pl](http://npsa-pbil.ibcp.fr/cgi-bin/secpred_hnn.pl)). The solid curve in Figure 4A indicated the denaturation of secondary structure in the buffer containing 4 M Gdn.HCl (Buffer E) (Fig. 4A, solid curve). Since the CD spectra were not measured below 190 nm (see Materials and Methods), estimations of the  $\beta$ -strand and random coil contents were deemed inaccurate and not presented (Johnson 1990). The addition of 5  $\mu$ M ifenprodil shifted the magnitudes of the spectra shown in Figure 4A (dashed curve). This shift demonstrated that Buffer 13-refolded soluble 6xHis-ATD2B indeed could bind ifenprodil. Experimentally measured changes in the  $\alpha$ -helical contents of 6xHis-ATD2B in the apo- (26.8%) and ifenprodil-bound (27.6%) forms were insignificant compared to the loop contents, which increased from 29.7% (apo-) to 34.7% (ifenprodil-bound).

**Table 2.** Theoretical and experimentally determined masses of peptides of 6xHis-ATD2B

	Molecular mass (Da)	
	Observed <sup>a</sup>	Calculated <sup>b</sup>
Intact 6xHis-ATD2B	46,839.30	47,464.20
N-terminal peptide sequencing peptides (post-thrombin cleavage)		
1 (16–22)	—	704.80
2 (54–61)	—	830.00
Trypsin-digested peptides		
1 (78–93)	1901.99	1900.92
2 (94–110)	1915.98	1915.01
3 (319–344)	2798.53	2797.43
4 (354–363)	1294.71	1293.66
5 (364–373)	1211.68	1210.63
6 (374–387)	1652.80	1651.73
7 (388–397)	1210.83	1209.78
8 (409–419)	1470.80	1469.75

<sup>a</sup> Molecular mass determined by MALDI TOF/TOF MS.

<sup>b</sup> Molecular mass calculated from the peptide sequences.

N-terminal sequencing (post-thrombin cleavage) was performed by Edman Sequencing (Midwest Analytical), and the trypsin-digested peptides were subjected to MALDI TOF/TOF MS analysis to obtain the peptide masses (Protein and Proteomics Centre, NUS, Singapore). Numbers in bracket denote the amino acid numbering (refer to Fig. 1B).

As the reported critical molecular determinants of ifenprodil binding to ATD of NR2B subunit are located within the soluble 6xHis-ATD2B protein, one should be able to obtain a dissociation constant ( $K_D$ ) for ifenprodil binding in a dose titration CD experiment. Buffer 13-refolded 6xHis-ATD2B but not the denatured 6xHis-ATD2B bound to ifenprodil in a dose-dependent manner at concentrations of 0.01–5  $\mu$ M as illustrated in Figure 4, B and C. The maximum shifts of magnitude at wavelength 219.6 nm indicated that ifenprodil bound to the soluble 6xHis-ATD2B with a  $K_D$  value of  $127.5 \pm 45$  nM ( $n = 4$ ).

## Discussion

Overexpression of the 6xHis-ATD2B fusion protein in *E. coli* yielded insoluble protein. Attempts to improve the yield of soluble protein by using lower temperatures (15°–25°C), different IPTG concentrations (0.4–1.0 mM) for varying lengths of induction time (2 h to overnight), and shorter ATD2B constructs did not help to improve the soluble expression of the protein (data not shown). Notably, overnight induction drastically decreased the amount of overexpressed 6xHis-ATD2B proteins.

Previously, Chen and Gouaux (1997) had successfully used a fractional factorial folding screen to determine the best refolding conditions for the production of the correctly folded and active S1S2 ligand binding domain of

the GluR2 AMPA receptor. We adapted the same refolding matrix screen, and we found that Buffer 13-refolded protein yielded the highest monomer:dimer ratio (2.33) and a very high percentage recovery (92.7%). Notably, Buffers 9 and 12 were ranked the next highest in the monomer:dimer ratios (1.99 and 1.90, respectively). Interestingly, the average hydrodynamic molecular weight of the soluble 6xHis-ATD2B was predicted to be 193 kDa, purporting a tetrameric species, from DLS analyses.

Our CD results suggested that the binding of ifenprodil induced conformational changes mainly at loop regions in the 6xHis-ATD2B protein. This observation is consistent with Asp101 and Phe176 (two critical molecular determinants for high-affinity binding of ifenprodil) being located at the loops linking  $\beta_3/\alpha_3$  and  $\beta_6/\alpha_6$  as reported by Perin-Dureau et al. (2002; see Fig. 4 therein). The  $K_D$  value of  $127.5 \pm 45$  nM for ifenprodil binding to 6xHis-ATD2B determined here corroborates with the reported  $IC_{50}$  values for functional NR1/NR2B receptors (Pahk and Williams 1997; Perin-Dureau et al. 2002).

Our study reinforces the conclusion that our 6xHis-ATD2B is folded into a homogenous, biologically relevant conformation, as this 6xHis-ATD2B (1) is soluble in aqueous solution as a monodispersed species, (2) possesses

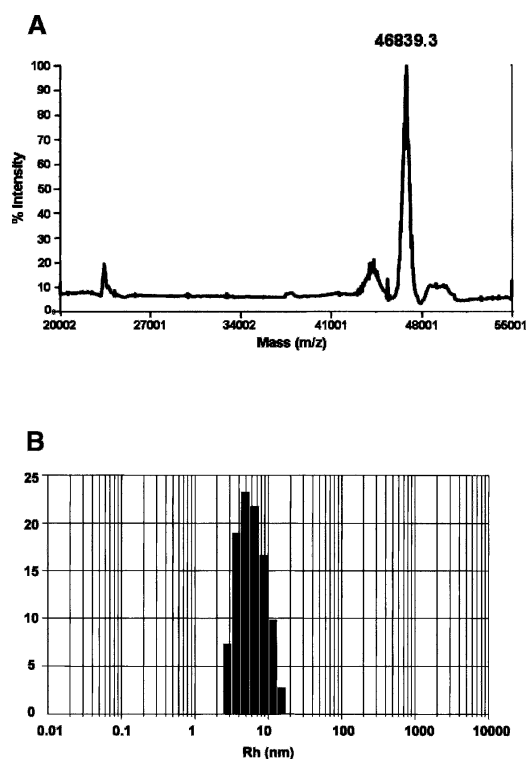


**Figure 3.** Characterization of 6xHis-ATD2B. (A) MALDI-TOF MS analysis of the 6xHis-ATD2B. The protein showed molecular mass of 46,839.3 Da. (B) Monodispersed species of 6xHis-ATD2B in Buffer 13 determined from DLS at 25°C.

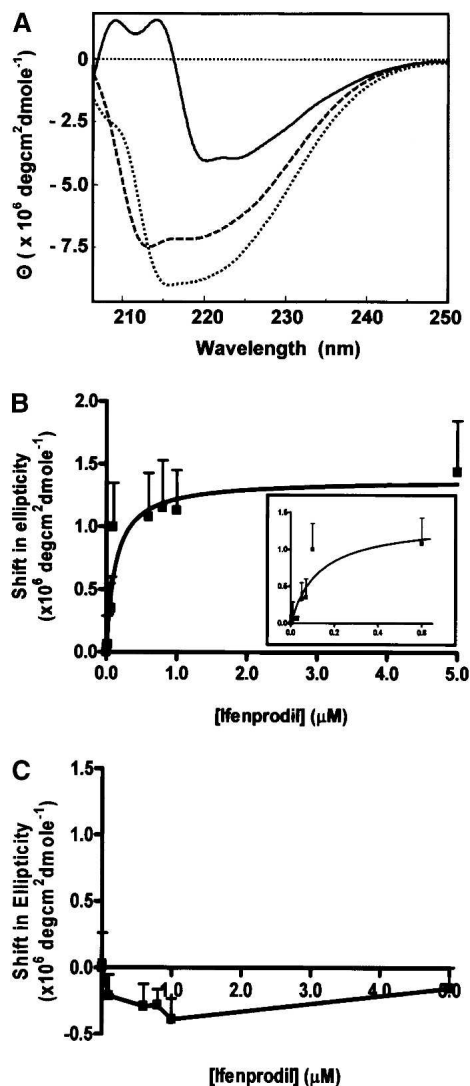


**Figure 4.** CD spectra of 6xHis-ATD2B proteins. (A) Solid curve represents denatured protein (in presence of 4 M Gdn.HCl); dotted curve represents Buffer 13-refolded 6xHis-ATD2B in the absence of ifenprodil; dashed curve represents in the presence 5  $\mu$ M ifenprodil. Note that 4 M Gdn.HCl did not generate absorbance between wavelengths recorded. (B) Ifenprodil dose titration curve. Buffer 13-refolded 6xHis-ATD2B showed a dose-dependent saturation with increasing concentrations of ifenprodil. (C) Denatured 6xHis-ATD2B showed no specific binding to ifenprodil throughout the range of concentrations studied. Each point represents the mean obtained from four experiments using proteins from at least two independent batches of induction and refolding. Error bars represent the standard error of the mean.

substantial secondary structure, and (3) is able to bind ifenprodil dose-dependently. This study is the first to assign a pharmacological binding constant to the isolated ATD of the NR2B subunit of NMDA receptors (127.5 nM) that is comparable to the corresponding binding constant obtained from [ $^3$ H]ifenprodil on rat cerebral cortex

(36.7 nM) (Schoemaker et al. 1990). In summary, we have presented several lines of evidence that support the conclusion that our soluble 6xHis-ATD2B protein is folded into a functional conformation that is useful for screening ATD-binding ligands and future structural investigations.

## Materials and methods

### Materials

The NMDA NR2B cDNA (U11419) clone was a gift from Dr. S.F. Heinemann (Salk Institute). pET30b(+)-EG plasmid was a gift from Dr. E. Gouaux (Columbia University). Restriction enzymes were purchased from New England Biolabs. Turbo and native *Pfu* polymerases were from Stratagene. T4 ligase was purchased from Promega. Thrombin used was from a thrombin cleavage capture kit (Novagen); lysozyme and DNase I were from Sigma. All primers designed were ordered from GibcoBRL and Genset. Ifenprodil tartrate and [R-(R\*,S\*)]- $\alpha$ -(4-Hydroxyphenyl)- $\beta$ -methyl-4-(phenylmethyl)-1-piperidine-propanol hydrochloride (RO 25-6981) were obtained from Sigma-Aldrich. 1,2-Diheptanoyl-sn-glycero-3-phosphocholine was from Avanti Polar Lipids. The 10,000 MWCO Slide-A-Lyzer Mini Dialysis Units (200  $\mu$ L) and Slide-A-Lyzer dialysis cassettes (12 mL) were purchased from Pierce. The anti-NR2B amino-terminal rabbit polyclonal antibody was purchased from Santa Cruz, and the anti-6xHis monoclonal antibody was from Clontech. For secondary antibodies, both the goat anti-rabbit and rabbit anti-mouse horseradish peroxidase antibodies were from Sigma-Aldrich. Protein molecular markers were from New England Biolabs. Antibiotics and chemicals of analytical and reagent grade were obtained from Sigma-Aldrich.

### Synthesis of ATD2B constructs for protein expression

To facilitate the cloning of the PCR-amplified insert of ATD2B using NcoI and XhoI on pET30b(+)-EG plasmid, the endogenous NcoI (Ile126–Gly128; amino acid numbering starts with first translated methionine) and XhoI (Leu199–Glu200) sites located within the ATD of the NR2B cDNA were removed using QuikChange site-directed mutagenesis as reported (Low et al. 2000). The primer pairs were H127Hf-2B, 5'-CATCCTGGGCATCCACGGGGGCTCATCTATG-3' and H127Hr-2B, 5'-CATAGATGAGCC C-CGTGGATGCCAGGATG-3'; L199Lf-2B, 5'-GTGGGC TGGGAGCTAGAGGAAGTCCTCT-G3' and L199 Lr-2B, 5'-CAGGAGGACTTCCTCTAGCTCCCAAGAGC-3'. The nicked double-stranded mutant DNA was transformed into XL2-Blue (heat-shocked 42°C  $\times$  45 sec) (Stratagene) or DH10B (electroporation) (Bio-Rad). Colonies were screened using restriction enzymes NcoI and/or XhoI for the abolishment of the corresponding site(s). The mutations were verified by dideoxy sequencing through the region of the mutations. Positive clones were designated as pcDNA1 NR2B(H127H/L199L).

The ATD2B gene encoding the R27–R393 amino acid residues of NMDA NR2B subunit was PCR-amplified from the pcDNA1 NR2B(H127H/L199L) plasmid using PfuTurbo polymerase (Stratagene). The sense primer 2B-PRM5 5'-TCCGAATTCCATGGCAGGTTCCCAAGAGC-3' and anti-sense primer 2B-PRM6 5'-GCGGCCGCTCGAGCCGAGGCCACACATAATAC-3' introduced NcoI and XhoI sites at the 5' and 3' ends of ATD2B (underlined). The PCR

reaction volume (100  $\mu$ L) contained template (20 ng), 200  $\mu$ g of each primer, 200  $\mu$ M dNTPs, 1 $\times$  PfuTurbo Buffer and 5 U PfuTurbo polymerase. The cycling conditions were 95°C  $\times$  1 min, 30 cycles of 95°C  $\times$  1 min, 55°C  $\times$  1 min, and 72°C  $\times$  2.5 min with a final 10-min extension at 72°C. The PCR yielded a single and specific amplicon of the predicted size. The amplicon was gel-purified (QIAquick Gel Extraction kit, QIAGEN). The full-length amplicon was sequenced to confirm identity. The NcoI-/XhoI-digested ATD2B amplicon was inserted downstream of the T7 promoter of pET30b(+)-EG expression vector via the NcoI and XhoI sites to create the recombinant pET30b(+)-EG-ATD2B plasmid. The amino terminus of ATD2B gene in pET30b(+)-EG-ATD2B plasmid was extended to encode the amino acid sequence MHHHHHH and a linker region containing cleavage recognition sites for thrombin and enterokinase during its construction (see Fig. 1). The authenticity of the full-length cloned inserts in all recombinant constructs was confirmed through restriction digestion and sequencing in both directions. pET30b(+)-EG ATD2B plasmid was transformed into BL21-CodonPlus-RIL (Stratagene) competent cells for protein expression.

### Buffers

Buffers used followed those detailed in Chen and Gouaux (1997) except for the ligand used:

Buffer A: 50 mM Tris HCl (pH 8.0), 1 mM EDTA, 100 mM NaCl, 1 mM phenylmethylsulfonyl fluoride (PMSF); B: 50 mM Tris HCl (pH 8.0), 10 mM EDTA, 100 mM NaCl, 0.5% Triton-X-100, 1 mM PMSF; C: 20 mM Tris HCl (pH 7.4), 1 mM EDTA, 200 mM NaCl, 1 mM PMSF; D: 50 mM Tris HCl (pH 7.4), 5 mM EDTA, 8 M guanidine hydrochloride (Gdn.HCl), 5 mM DTT; E: 20 mM NaOAc, 4 M Gdn.HCl, 1 mM EDTA, 1 mM DTT (pH 4.5); F: 100 mM sodium phosphate (pH 6.8), 200 mM sodium sulfate, 10  $\mu$ M RO 25-6981, 1 mM DTT, 2 mM EDTA; 2: 20 mM Tris HCl (pH 7.4), 1 mM EDTA, 200 mM NaCl; 13: 10 mM NaCl, 0.4 mM KCl, 2.0 mM KCl, 2.0 mM CaCl<sub>2</sub>, 500 mM L-arginine hydrochloride, 20% glycerol, 1% sucrose, 750 mM Gdn.HCl, 1 mM DTT.

### Expression of 6xHis-ATD2B

For expression of 6xHis-ATD2B on a 1-L scale, 100 mL of overnight seed cultures was added to 1 L of fresh Luria-Bertani (LB) media and incubated at 37°C until OD<sub>600</sub> 0.8–1.0 before induction with 0.5 mM IPTG and incubated at 37°C for another 5 h. The 6xHis-ATD2B induced cells were harvested at 3500 rpm  $\times$  20 min at 4°C. Cell pellets were washed once with 1  $\times$  PBS (pH 7.4). The expression of recombinant protein in *E. coli* was analyzed by SDS-PAGE.

The cell pellet expressing the 6xHis-ATD2B was resuspended in 30 mL of Buffer A supplemented with 0.3 mg/mL lysozyme, 17  $\mu$ g/mL DNase I, 1 mM PMSF, and 2 mM CaCl<sub>2</sub>. The cell suspensions were then incubated on ice for 20 min before lysis using sonication (Vibra Cell VC130, Sonics) or passing through the French Pressure Cell (ThermoSpectronic) twice at 15,000 psi on a 40-K cell. The resultant cell lysate was centrifuged at 23,000g at 4°C for 20 min. The crude inclusion bodies were washed with 25 mL of ice-cold Buffer B followed by 25 mL of ice-cold Buffer C, both containing 1 mM PMSF. The washed inclusion bodies were then solubilized in 9 mL Buffer D containing 5 mM DTT with stirring at room

temperature for 6 h or until the inclusion bodies became clear. The solubilized solution was clarified by centrifugation at 42,700 rpm at 4°C for 30 min, and the resultant supernatant was diluted with 28 mL ice-cold Buffer E containing 1 mM DTT in a dropwise manner with stirring at 4°C. The resultant solution was centrifuged at 42,700 rpm at 4°C for 1 h. The supernatant containing the soluble and refolded protein was carefully aliquoted out for further investigation or stored at –80°C.

### Affinity Ni<sup>2+</sup>-column purification of 6xHis-ATD2B under denaturing conditions

The solubilized supernatant of 6xHis-ATD2B in Buffer E was loaded into a Ni<sup>2+</sup>-charged HiTrap HP 5 mL column (Amersham) pre-equilibrated with binding buffer (10 mM Na<sub>2</sub>HPO<sub>4</sub>, 10 mM NaH<sub>2</sub>PO<sub>4</sub>, 500 mM NaCl [pH 7.4]) and was allowed to bind for 2 h at 4°C. The column was washed with washing buffers containing increasing concentrations of imidazole (20–150 mM). Elution was done using an elution buffer (10 mM Na<sub>2</sub>HPO<sub>4</sub>, 10 mM NaH<sub>2</sub>PO<sub>4</sub>, 500 mM NaCl [pH 7.4]) containing 300 mM imidazole.

### 16 refolding matrix screen

First, 200  $\mu$ L of affinity-purified 6xHis-ATD2B in Buffer E at the starting protein concentration of either 0.1 mg/mL or 1.0 mg/mL was dialyzed against 17 mL of the 16 refolding buffers in Slide-A-Lyzer Mini Dialysis Units at either 4°C or room temperature for 18 h with one change of buffer (Chen and Gouaux 1997). Thereafter, the resultant dialyzed samples were dialyzed against 40 mL of Buffer F at 4°C for 4 h. The final protein samples were centrifuged at 50,000 rpm for 45 min at 4°C. The volume of recovered protein in each refolding condition was recorded, and the percentage of recovery was calculated. Monomeric and dimeric forms of the protein solutions were analyzed using native PAGE (Gallagher 1995) and visualized using silver staining (BioRad). The proportions of the monomers and dimers and the percentage yield of the proteins were then measured using densitometry.

### Sample preparation for CD analyses

The affinity-purified protein in Buffer E was concentrated to 0.2 mg/mL (Centricon Plus-70, Millipore). Next, 12 mL of 0.2 mg/mL protein was dialyzed against 1 L of Buffer 2 for 48 h with extensive changes of buffer using a Slide-A-Lyzer 12-mL dialysis cassette (Pierce). It was then refolded in Buffer 13 at 4°C for 18 h with one change of buffer. Thereafter the refolded proteins were dialyzed against Buffer 2 at 4°C for 48 h with multiple changes of buffer. The final protein sample was centrifuged at 50,000 rpm for 45 min at 4°C. To facilitate the comparison of data, all of the protein samples (in final buffer 2) were concentrated to 1 mg/mL using a Vivaspin 2 mL concentrator (Vivascience) for CD characterization and DLS analyses.

### CD measurements and secondary structure composition estimation

The CD measurements were performed at 25°C using a Jasco J-715 spectropolarimeter equipped with a 1.0-mm path-length

cuvette. The samples were scanned from 190 to 250 nm and accumulated 10 times at a resolution of 0.1 nm with a scanning speed of 50 nm/min and sensitivity of 200 mdeg. All of the CD data are expressed as molar ellipticity. The protein secondary structures were estimated using the software J-700 for Windows Secondary Structure Estimation, version 1.10.02 (Jasco Corp.). Due to the lack of a cuvette with path length 0.1 mm and the high NaCl concentration in final Buffer 2 (exceeding the manufacturer's recommendation of 100 mM NaCl), no CD was recorded below 190 nm, and hence  $\beta$ -strand and random coil contents were not determined experimentally.

#### Modulator binding assay determined by CD

Increasing amounts of ifenprodil were added in small aliquots from stock solutions to 350  $\mu$ L of protein solution and were allowed to bind for 35 min at room temperature. The CD spectra of the protein in the absence and presence of increasing concentrations of ifenprodil (0.01–5  $\mu$ M) were recorded. The final change of assay volume was < 3%. Duplicates were obtained per batch of induced/refolded 6xHis-ATD2B. Dose-titrations of ifenprodil binding to 6xHis-ATD2B were determined in two separate batches of induced/refolded proteins.

#### DLS measurements

DLS measurements were made with a DynaPro instrument (Protein Solutions). Each sample was centrifuged for 20 min at 13,200 rpm before being aliquoted into the 12  $\mu$ L-quartz cuvette of path length 1.5 mm. Measurements were made in duplicate at 25°C for each sample. The hydrodynamic molecular weights were calculated using Dynamic V5 software (Protein Solutions).

#### Measurement of protein concentration

The protein concentration of purified 6xHis-ATD2B was determined by the Bradford protein assay and the absorbance at 280 nm (GeneQuant Pro, Amersham Biosciences) using an extinction coefficient ( $\epsilon_{280} = 60,430 \text{ M}^{-1}\text{cm}^{-1}$ ) calculated from the amino acid sequence using the ProtParam Web site (<http://tw.expasy.org/tools/protparam.html>).

#### SDS-PAGE, immunoblotting, densitometry, and mass spectrometry

The proteins were separated by denaturing SDS-PAGE according to the method of Laemmli, using a Hoefer Mighty Small Vertical Electrophoresis System. They were analyzed on 15% polyacrylamide gels stained using Coomassie Brilliant Blue R-250. For Western blotting, the proteins were electrophoresed and transferred to nitrocellulose or PVDF membranes. The membranes were blocked with 5% nonfat milk and subsequently probed with either anti-ATD2B (1:500 dilution) or anti-6xHis (1:10,000 dilution) primary antibody. Detection of the primary antibody was performed with anti-rabbit IgG horseradish peroxidase (HRP) (1 mg/mL) followed by ECL Plus Western blotting detection reagents (Amersham Pharmacia). Densitometric analysis was done using the SynGene Multi Genius Bio Imaging System. The relative band intensity was analyzed using Gene Tools software (version 3.05). The MALDI-TOF MS analysis was performed using

Voyager DE-STR (Applied Biosystems) to determine the molecular weight of 6xHis-ATD2B. In addition, 0.5  $\mu$ g of protein was desalted using Zip Tip<sub>C4</sub> pipette tips (Millipore) before the MS analysis. A MALDI-TOF/TOF MS analysis was performed to obtain the masses and sequences of the trypsin-digested peptides. Here, 0.5  $\mu$ g of 6xHis-ATD2B was digested using 0.25  $\mu$ g of trypsin and analyzed using the 4700 Proteomic Analyzer (Applied Biosystems). Both the molecular weight of the protein and the sequences of the trypsin-digested peptides were analyzed using Data Explorer software. Amino-terminal sequencing (Midwest Analytical) was performed using protein sequencers Perkin-Elmer Applied Biosystems.

#### Data analysis

The shift in ellipticity of the CD spectra at 219.6 nm (where the signal change on ifenprodil binding was maximal) was calculated. The experimental data were analyzed by nonlinear curve fitting (GraphPad Prism).

#### Acknowledgments

We thank Drs. S.F. Heinemann and E.G. Gouaux for supplying the NR2B cDNA and pET30b(+)-EG vector, respectively; Drs. Henry Y-K. Mok and J. Sivaraman for their valuable advice on CD and DLS analyses; and Ms. S-K. Goh for technical help. We are grateful to Drs. Xiaodong Cheng, Xing Zhang, and John R. Hepler from the Departments of Biochemistry and Pharmacology, Emory University, for their insightful suggestions and encouragement. The Department of Biological Sciences, National University of Singapore, is acknowledged for the use of DynaPro DLS. We thank Dr. Alvin Teo for his critical reading of the manuscript. Part of this work was done in the National Neuroscience Institute where C.M.L. was a Principal Investigator in the Glutamate Receptor Laboratory. Support for this research was provided by NIH NS39419 (S.F.T.) and Singapore NMRC 05812001 (C.M.L.). F.M.N. is the recipient of a graduate research scholarship from the National University of Singapore.

#### References

- Chen, G.Q. and Gouaux, E. 1997. Overexpression of a glutamate receptor (GluR2) ligand binding domain in *Escherichia coli*: Application of a novel protein folding screen. *Proc. Natl. Acad. Sci.* **94**: 13431–13436.
- Dingledine, R., Borges, K., Bowie, D., and Traynelis, S.F. 1999. The glutamate receptor ion channels. *Pharmacol. Rev.* **51**: 7–61.
- Dirnagl, U., Iadecola, C., and Moskowitz, M.A. 1999. Pathobiology of ischemic stroke: An integrated view. *Trends Neurosci.* **22**: 391–397.
- Furukawa, H. and Gouaux, E. 2003. Mechanisms of activation, inhibition and specificity: Crystal structures of the NMDA receptor NR1 ligand-binding core. *EMBO J.* **22**: 2873–2885.
- Gallagher, S. 1995. Electrophoresis. In *Current protocols in protein science* (ed. J.E. Coligan), pp. 10.3.4. Wiley, New York.
- Gallagher, M.J., Huang, H., Pritchett, D.B., and Lynch, D.R. 1996. Interactions between ifenprodil and the NR2B subunit of the N-methyl-D-aspartate receptor. *J. Biol. Chem.* **271**: 9603–9611.
- Gallagher, M.J., Huang, H., Grant, E.R., and Lynch, D.R. 1997. The NR2B-specific inter-actions of polyamines and protons with the N-methyl-D-aspartate receptor. *J. Biol. Chem.* **272**: 24971–24979.
- Johnson, W.C.J. 1990. Protein secondary structure and circular dichroism: A practical guide. *Proteins* **7**: 205–214.
- Krupp, J.J., Vissel, B., Heinemann, S.F., and Westbrook, G.L. 1998. N-terminal domains in the NR2 subunit control desensitization of NMDA receptors. *Neuron* **20**: 317–327.

- Kunishima, N., Shimada, Y., Tsuji, Y., Sato, T., Yamamoto, M., Kumasaka, T., Nakanishi, S., Jingami, H., and Morikawa, K. 2000. Structural basis of glutamate recognition by a dimeric metabotropic glutamate receptor. *Nature* **7**: 971–977.
- Lee, J.M., Zipfel, G.J., and Choi, D.W. 1999. The changing landscape of ischemic brain injury mechanisms. *Nature* **399**: A7–A14.
- Low, C.-M., Zheng, F., Lyuboslavsky, P., and Traynelis, S.F. 2000. Molecular determinants of coordinated proton and zinc inhibition of N-methyl-D-aspartate NR1/NR2A receptors. *Proc. Natl. Acad. Sci.* **97**: 11062–11067.
- Masuko, T., Kashiwagi, K., Kuno, T., Nguyen, N.D., Pahk, A.J., Fukuchi, J., Igarashi, K., and Williams, K. 1999. A regulatory domain (R1-R2) in the amino terminus of the N-methyl-D-aspartate receptor: Effects of spermine, protons, and ifenprodil, and structural similarity to bacterial leucine/isoleucine/valine binding protein. *Mol. Pharmacol.* **55**: 957–969.
- Meddows, E., Le Bourdelles, B., Grimwood, S., Wafford, K., Sandhu, S., Whiting, P., and McIlhinney, R.A. 2001. Identification of molecular determinants that are important in the assembly of N-methyl-D-aspartate receptors. *J. Biol. Chem.* **276**: 18795–18803.
- Meldrum, B.S., Akbar, M.T., and Chapman, A.G. 1999. Glutamate receptors and transporters in genetic and acquired models of epilepsy. *Epilepsy Res.* **36**: 189–204.
- Nakanishi, N., Schneider, N.A., and Axel, R. 1990. A family of glutamate receptor genes: Evidence for the formation of heteromultimeric receptors with distinct channel properties. *Neuron* **5**: 569–581.
- Obrenovitch, T.P. and Urenjak, J. 1997. Is high extracellular glutamate the key to excitotoxicity in traumatic brain injury. *J. Neurotrauma* **14**: 677–698.
- Paas, Y. 1998. The macro- and microarchitectures of the ligand-binding domain of glutamate receptors. *Trends Neurosci.* **21**: 117–125.
- Pahk, A.J. and Williams, K. 1997. Influence of extracellular pH on inhibition by ifenprodil at N-methyl-D-aspartate receptors in *Xenopus* oocytes. *Neurosci. Lett.* **225**: 29–32.
- Paoletti, P., Perin-Dureau, F., Fayyazuddin, A., Le Goff, A., Callebaut, I., and Neyton, J. 2000. Molecular organization of a zinc binding N-terminal modulatory domain in a NMDA receptor subunit. *Neuron* **28**: 911–925.
- Perez-Otano, I., Schulteis, C.T., Contractor, A., Lipton, S.A., Trimmer, J.S., Sucher, N.J., and Heinemann, S.F. 2001. Assembly with the NR1 subunit is required for surface expression of NR3A-containing NMDA receptors. *J. Neurosci.* **21**: 1228–1237.
- Perin-Dureau, F., Rachline, J., Neyton, J., and Paoletti, P. 2002. Mapping the binding site of the neuroprotectant ifenprodil on NMDA receptors. *J. Neurosci.* **22**: 5955–5965.
- Schoemaker, H., Allen, J., and Langer, S.Z. 1990. Binding of [<sup>3</sup>H]ifenprodil, a novel antagonist, to a polyamine-sensitive site in the rat cerebral cortex. *Eur. J. Pharmacol.* **176**: 249–250.
- Villarroya, A., Regalado, M.P., and Lerma, J. 1998. Glycine-independent NMDA receptor desensitization: Localization of structural determinants. *Neuron* **20**: 329–339.
- Wo, Z.G. and Oswald, R.E. 1995. A topological analysis of goldfish kainite receptors predicts three transmembrane segments. *J. Biol. Chem.* **270**: 2000–2009.
- Zheng, F., Erreger, K., Low, C.-M., Banke, T., Lee, C.J., Conn, P.J., and Traynelis, S.F. 2001. Allosteric interaction between the amino terminal domain and the ligand binding domain of NR2A. *Nat. Neurosci.* **4**: 894–901.